HHS Public Access

Author manuscript

J Bioenerg Biomembr. Author manuscript; available in PMC 2016 November 07.

Published in final edited form as:

J Bioenerg Biomembr. 2016 June ; 48(3): 175–188. doi:10.1007/s10863-016-9644-1.

Mg^{2+} differentially regulates two modes of mitochondrial Ca^{2+} uptake in isolated cardiac mitochondria: implications for mitochondrial Ca^{2+} sequestration

Christoph A. Blomeyer[1], **Jason N. Bazil**[2,3,4], **David F. Stowe**[1,4,5,6], **Ranjan K. Dash**[3,4,5], and **Amadou K. S. Camara**[1]

Amadou K. S. Camara: aksc@mcw.edu

[1]Department of Anesthesiology, Medical College of Wisconsin, 8701 Watertown Plank Road, Milwaukee, WI 53226, USA

[2]Department of Molecular and Integrative Physiology, University of Michigan, Ann Arbor, MI 48109, USA

[3]Biotechnology and Bioengineering Center, Medical College of Wisconsin, Milwaukee, WI 53226, USA

[4]Department of Physiology, Medical College of Wisconsin, Milwaukee, WI 53226, USA

[5]Department of Biomedical Engineering, Marquette University, Milwaukee, WI 53233, USA

[6]Research Service, Zablocki Veterans Affairs Medical Center, Milwaukee, WI 53295, USA

Abstract

The manner in which mitochondria take up and store Ca^{2+} remains highly debated. Recent experimental and computational evidence has suggested the presence of at least two modes of Ca^{2+} uptake and a complex Ca^{2+} sequestration mechanism in mitochondria. But how Mg^{2+} regulates these different modes of Ca^{2+} uptake as well as mitochondrial Ca^{2+} sequestration is not known. In this study, we investigated two different ways by which mitochondria take up and sequester Ca^{2+} by using two different protocols. Isolated guinea pig cardiac mitochondria were exposed to varying concentrations of $CaCl_2$ in the presence or absence of $MgCl_2$. In the first protocol, A, $CaCl_2$ was added to the respiration buffer containing isolated mitochondria, whereas in the second protocol, B, mitochondria were added to the respiration buffer with $CaCl_2$ already present. Protocol A resulted first in a fast transitory uptake followed by a slow gradual uptake. In contrast, protocol B only revealed a slow and gradual Ca^{2+} uptake, which was approximately 40 % of the slow uptake rate observed in protocol A. These two types of Ca^{2+} uptake modes were differentially modulated by extra-matrix Mg^{2+}. That is, Mg^{2+} markedly inhibited the slow mode of Ca^{2+} uptake in both protocols in a concentration-dependent manner, but not the fast mode of

Correspondence to: Amadou K. S. Camara, aksc@mcw.edu.

Christoph A. Blomeyer and Jason N. Bazil equally contributed to the work.

This work was presented in podium form at the 2014 Biophysical Society meeting: Blomeyer CA, Bazil JN, Stowe DF, Dash RK, and Camara AKS. The potential for another calcium uptake mode in cardiac mitochondria. Biophysical Society Meeting, San Francisco, Feb. 15–19, 2014. [Biophys J 106(2), p.242a]

Electronic supplementary material The online version of this article (doi:10.1007/s10863-016-9644-1) contains supplementary material, which is available to authorized users.

uptake exhibited in protocol A. Mg^{2+} also inhibited Na^{+}-dependent Ca^{2+} extrusion. The general Ca^{2+} binding properties of the mitochondrial Ca^{2+} sequestration system were reaffirmed and shown to be independent of the mode of Ca^{2+} uptake, i.e. through the fast or slow mode of uptake. In addition, extra-matrix Mg^{2+} hindered Ca^{2+} sequestration. Our results indicate that mitochondria exhibit different modes of Ca^{2+} uptake depending on the nature of exposure to extra-matrix Ca^{2+}, which are differentially sensitive to Mg^{2+}. The implications of these findings in cardiomyocytes are discussed.

Keywords

Mitochondria; Cardiac; Calcium uptake; Calcium sequestration; Calcium efflux

Introduction

Mitochondria have the capacity to take up and sequester large amounts of Ca^{2+} (Vasington and Murphy 1962). For decades it was believed that mitochondrial Ca^{2+} was a necessary means to maintain proper energy balance in the heart. However, recent mitochondrial Ca^{2+} uniporter (MCU) knockout studies in mice have contested the importance of Ca^{2+} in mitochondrial energy homeostasis (Pan et al. 2013). Cardiac specific MCU knockout studies using a mouse model reveal that cardiac mitochondrial Ca^{2+} is only essential during high stress conditions, but not for routine activities (Kwong et al. 2015; Luongo et al. 2015; Wu et al. 2015). Whereas the role of mitochondria as a Ca^{2+} sink against cytosolic Ca^{2+} overload is well recognized (Szabadkai and Duchen 2008; Nicholls 2005; Rasola and Bernardi 2011), their role in shaping the cytosolic Ca^{2+} transients during physiological conditions is still debated (Boyman et al. 2014; Lu et al. 2013). Moreover, the precise mechanisms and consequences by which mitochondria take up, extrude, and sequester cytosolic Ca^{2+} remain obscure.

It has been suggested that mitochondrial Ca^{2+} uptake consists of different components that result in different matrix free Ca^{2+} dynamics. One possible component constitutes the rapid and beat-to-beat changes in the concentration of matrix free Ca^{2+} ($[Ca^{2+}]_m$) (Dedkova and Blatter 2013; Huser et al. 2000). This fast mode of Ca^{2+} uptake is proposed to be responsible for regulating ATP production (Dedkova and Blatter 2013; Carafoli 2010; Tarasov et al. 2012) by altering activities of Ca^{2+}-sensitive dehydrogenases and other Ca^{2+}-sensitive processes. However, this idea, as noted above, is controversial based on recent data obtained from MCU knockout mice (Pan et al. 2013; Kwong et al. 2015). Another possible component that has been proposed is the slow mode of Ca^{2+} uptake, which functions as a low-pass filter of the cytosolic Ca^{2+} transient while gradually accumulating matrix Ca^{2+} (Dedkova and Blatter 2013; Sedova et al. 2006). It is also thought to be a significant source of Ca^{2+} uptake during periods of sustained elevation of cytosolic Ca^{2+} (Carafoli 2010; Dorn and Maack 2013), such as in ischemia and reperfusion (IR) injury (Varadarajan et al. 2001).

The MCU is the primary pathway for Ca^{2+} uptake (Baughman et al. 2011; De Stefani et al. 2011) and may possess multiple conductance modes (Kirichok et al. 2004; Wei et al. 2012; Csordas et al. 2013). The recent identities of the MCU channel and its regulatory proteins

(e.g. MICU1 and MICU2) involved in modulating mitochondrial Ca^{2+} uptake are now characterized as sensors of extra-matrix $[Ca^{2+}]$ ($[Ca^{2+}]_e$) that stimulate or inhibit MCU, respectively. This would allow for a rapid response of mitochondria to Ca^{2+} signals generated in the cytoplasm (Marchi and Pinton 2014). Previous studies suggest that there exist additional potential Ca^{2+} uptake modes: the mitochondrial ryanodine-like receptor (Beutner et al. 2001; Tewari et al. 2014) and the rapid-mode (RaM) of Ca^{2+} uptake (Buntinas et al. 2001; Gunter et al. 1998; Sparagna et al. 1995). These fast modes of Ca^{2+} uptake were postulated, but not conclusively shown, to be responsible for transduction of physiological Ca^{2+} transients to match oxidative phosphorylation with energetic demands (Huser et al. 2000; O'Rourke and Blatter 2009).

Pharmacological inhibitors and/or modeling approaches have been used to identify the different modes of Ca^{2+} uptake, but the conclusions drawn from these studies have been disputed. For example, recent studies show relatively little mitochondrial Ca^{2+} uptake during physiological Ca^{2+} transients (Boyman et al. 2014; Lu et al. 2013), which implies that in the physiological setting, MCU might play only a negligible role in shaping physiological Ca^{2+} dynamics in the beating heart. Moreover, when mitochondria are loaded with sufficient Ca^{2+}, changes in matrix free Ca^{2+} are difficult to detect due to the higher buffering power associated with higher mitochondrial Ca^{2+} loads (Bazil et al. 2013; Blomeyer et al. 2013). Regardless, the MCU becomes most relevant when cytosolic $[Ca^{2+}]$ is abnormally elevated, such as during IR, oxidative stress, sarcoplasmic reticulum stress, or Ca^{2+} overload (Varadarajan et al. 2001; An et al. 2001a; Rhodes et al. 2003; An et al. 2001b).

Excess Ca^{2+} uptake by mitochondria is sequestered in a phosphate-dependent reaction that forms amorphous calcium phosphate (CaPi) granules (Chalmers and Nicholls 2003; Greenawalt et al. 1964; Kristian et al. 2007). The exact composition of these CaPi granules is unknown, but they are presumed to consist of mixtures of $Ca_3(PO_4)_2$, $Ca_8H_2(PO_4)_6$, and $Ca_{10}(PO_4)_6(OH)_2$ (Thomas and Greenawalt 1968). The properties of this sequestration system are a current area of interest because the buffering system alters both Ca^{2+} uptake and release dynamics (Blomeyer et al. 2013), and may regulate mitochondrial permeability transition (mPTP) (Szabadkai and Duchen 2008; Wei et al. 2012), which in turn may regulate mitochondrial Ca^{2+} transients (Sareen et al. 2007). In the heart and other excitatory tissues, the mitochondrial Na^+/Ca^{2+} exchanger (mNCE) is the primary pathway for Ca^{2+} extrusion (Boyman et al. 2013; Cai and Lytton 2004; Palty et al. 2004). Therefore, $[Ca^{2+}]_m$ is primarily maintained by a balance of Ca^{2+} uptake facilitated by the MCU, Ca^{2+} extrusion by the mNCE, and Ca^{2+} buffering by the sequestration system. The sequestration system acts as a Ca^{2+} reservoir so that the activities of MCU and mNCE establish a set point that helps maintain sub-lethal thresholds of cytosolic Ca^{2+} during Ca^{2+} loading conditions.

Thus, the modes of mitochondrial Ca^{2+} uptake and their regulation remain obscure. Interestingly, in a recent study, we reported that mitochondrial Ca^{2+} uptake displays two different profiles of matrix Ca^{2+} transient when $CaCl_2$ was added to mitochondrial suspension: a fast uptake of Ca^{2+} followed by a slower and more gradual uptake as matrix Ca^{2+} plateaus to a steady state (Boelens et al. 2013). Addition of Mg^{2+} to the respiration buffer appeared to have a differential effect on the two phases of the Ca^{2+} transient, with the slow phase attenuated more than the fast uptake phase. However, the impact of Mg^{2+} on

mitochondria buffering of Ca^{2+} is not known. In the present study, we used a non-pharmacological approach to distinguish a slow and fast mode of mitochondrial Ca^{2+} uptake and determine the impact of extra-matrix Mg^{2+} on the modes of Ca^{2+} uptake and the mitochondrial buffering capacity or sequestration power of Ca^{2+}. To further delineate the two modes of Ca^{2+} uptake, mitochondria were exposed to two different protocols based on the order by which mitochondria or $CaCl_2$ were first added to the respiration buffer with and without added $MgCl_2$.

Methods

Mitochondrial isolation

All experiments conformed to the Guide for the Care and Use of Laboratory Animals, and were approved by the Medical College of Wisconsin Institutional Animal Care and Use Committee. Mitochondria from guinea pig hearts were isolated as previously described (Blomeyer et al. 2013; Boelens et al. 2013; Aldakkak et al. 2013; Haumann et al. 2010). Briefly, guinea pigs (250–350 g) were anesthetized with intraperitoneal injection of 30 mg ketamine, and 700 units of heparin for anticoagulation. Hearts were excised and minced in ice-cold isolation buffer containing 200 mM mannitol, 50 mM sucrose, 5 mM KH_2PO_4, 5 mM MOPS, 1 mM EGTA and 0.1 % bovine serum albumin (BSA). Buffer pH was adjusted to 7.15 with KOH. The minced pieces were suspended in 2.65 ml ice-cold buffer with 5 U/ml protease (from *Bacillus licheniformis*) and homogenized at low speed for 30 s. Afterwards, 17 ml of ice-cold isolation buffer was added, and the suspension was again homogenized for 30 s and centrifuged at 8000 *g* for 10 min. The supernatant was discarded, and the pellet was re-suspended in 25 ml of ice-cold isolation buffer and centrifuged at 900 *g* for 10 min. The supernatant was recovered and centrifuged once more at 8000 *g* to yield the final mitochondrial pellet, which was re-suspended in isolation buffer and kept on ice (4 °C) for experiments after fluorescent dye loading to measure matrix Ca^{2+} transients.

The mitochondrial protein concentration was measured using the Bradford method (1976) and diluted with isolation buffer to a protein concentration of 5 mg/ml and incubated with the appropriate fluorescent dye or the vehicle (DMSO). Incubated mitochondria were re-suspended in 25 ml of ice-cold isolation buffer and re-centrifuged at 8000 *g*. Subsequently, the dye-loaded pellet was re-suspended in cold isolation buffer, and the protein concentration was measured again using the Bradford method and diluted finally to 12.5 mg/ml. The final mitochondrial suspension was kept in packed ice (4 °C), and all subsequent experiments were conducted within 6 h after the last step of the isolation procedure.

Experimental groups and protocols

Isolated mitochondria were exposed to five different concentrations of $CaCl_2$ and three different concentrations of $MgCl_2$. In addition, each of these groups was exposed to two different Ca^{2+} loading protocols, resulting in 30 groups overall. The only difference between the two experimental protocols (A and B) was the order of addition of mitochondria and $CaCl_2$ to the respiration buffer containing pyruvic acid. Extra-matrix (buffer) free Ca^{2+} ($[Ca^{2+}]_e$) and matrix free Ca^{2+} ($[Ca^{2+}]_m$) were monitored under identical experimental conditions for both protocols, except for the order of addition of $CaCl_2$ or mitochondria to

the buffer. For the NADH and $\Delta\Psi_m$ measurements, the number of experimental groups was reduced to eight for each experimental protocol (A and B). Each experiment was conducted with mitochondria pooled from 2 hearts and repeated 3–4 times on different days. Respiration buffer, which was adjusted to pH 7.15 with KOH, contained 130 mM KCl, 5 mM K_2HPO_4, 20 mM MOPS, 0.1 % BSA, and 40 μM EGTA (Blomeyer et al. 2013; Haumann et al. 2010). The mitochondrial concentration for all experiments was 0.5 mg/mL. The pH of the respiratory buffer remains at 7.15 after the addition of $CaCl_2$ and other substances, which was verified using a self-calibrating pH meter at the end of each experiment.

All experiments were conducted at room temperature (25 °C) using the cuvette-based fluorescence spectrophotometer described in our previous studies (Blomeyer et al. 2013; Boelens et al. 2013; Haumann et al. 2010; Agarwal et al. 2012, 2014; Aldakkak et al. 2011). Pyruvic acid (PA, 0.5 mM), cyclosporine A (CsA, 0.5 μM) and $MgCl_2$ (0, 0.5, 1.0 mM) were always present in the buffer. Ruthenium red (RR, 1 μM) was added at 300 s after all of the Ca^{2+} bolus was taken up. The volume of the experimental buffer in the cuvette containing no added EGTA, and before adding any substance was 910 μL. The volume of added substances (PA, $MgCl_2$, $CaCl_2$, CsA, NaCl) to the cuvette was 10 μL each and the volume of the mitochondrial suspension added to the cuvette was 40 μL resulting in a total volume of 1000 μl for each experiment in protocols A and B. At a final volume of 1000 μL, the dilution factor after the addition of mitochondria was 25 times. Since the initial concentration of mitochondria following isolation was 12.5 mg/mL, the final mitochondrial suspension was 0.5 mg/mL in each experiment. The addition of a 40 μL volume of mitochondrial suspension, which had a concentration of 1 mM EGTA from the original mitochondrial suspension (12.5 mg/mL), resulted in a final EGTA concentration of approximately 40 μM for the mitochondrial suspension in the cuvette. The experimental buffer had a $[Ca^{2+}]_e$ of approximately 50 nM that was similar to $[Ca^{2+}]_m$ before adding any $CaCl_2$.

The protocols (A and B) used to assess differences in $[Ca^{2+}]$ dynamics are shown in Fig.1. In protocol A at $t = 30$ s, 40 μL mitochondrial suspension was added to the experimental buffer. At $t = 60$ s, 0, 10, 20, 30 or 40 μM total $CaCl_2$ (10 μL of concentrated solution) was added to the mitochondrial suspension. In protocol B at $t = 30$ s, 0, 10, 20, 30 or 40 μM total $CaCl_2$ (10 μL of concentrated solution) was added first to the experimental buffer followed by addition of 40 μL mitochondrial suspension at $t = 60$ s. A high-speed magnetic stirring bar was turned on at the onset of each experiment to ensure prompt and rapid continuous mixing of the cuvette contents. With this approach, the effect of high initial localized boluses of $[CaCl_2]$ on mitochondria in protocol A was minimized. In both protocols at $t = 300$ s, 1 μM RR was added to block the MCU and to prevent Ca^{2+} re-uptake after its release via the NCE. At $t = 360$ s, 10 mM NaCl was added to induce Ca^{2+} efflux. The respiration buffer including the added PA was Na^+-free, except for the NaCl added at the end of each protocol to elicit Ca^{2+} release via mNCE activation. To avoid differences in buffer volume, the vehicle (deionized H_2O) was used for 0 mM $MgCl_2$ and 0 μM $CaCl_2$. Some additional experiments (not shown) were conducted in the presence of the mNCE inhibitor, CGP-37,157 (25 μM; Tocris Bioscience, Minneapolis, MN), to verify that the observed Na^+-induced Ca^{2+} efflux was due only to mNCE activity. All chemicals were obtained from Sigma-Aldrich (St. Louis, MO) unless noted otherwise.

Assessment of mitochondrial functional integrity

Before and after fluorescence measurements were made using the PTI spectrofluorometer, mitochondrial functional integrity/viability was assessed by measuring the respiratory control index (RCI) with a Clark type O_2 electrode (MT200A, Strathkelvin Instruments, Glasgow, UK). The RCI of mitochondria energized with 0.5 mM PA was calculated by dividing the rate of state 3 respiration (250 μM ADP) by the rate of state 4 respiration. Before the start of fluorescent measurements, RCI values were above 12 and at the end of the measurements (after approximately 6 h) RCI values were revaluated and remained above 8. This strong RCI after 6 h indicates that the mitochondria were viable and well coupled for the duration of the experiments.

Fluorescence measurements

Fluorescence spectrophotometry (Qm-8, Photon Technology International, Birmingham, NJ) was used to assess levels of $[Ca^{2+}]_e$ and $[Ca^{2+}]_m$, $\Delta\Psi_m$, and NADH. Fura-4F (Invitrogen™, Eugene, OR) was used to measure either $[Ca^{2+}]_m$ (AM form) or $[Ca^{2+}]_e$ (penta-potassium salt). For $[Ca^{2+}]_m$ measurements, mitochondria were incubated for 30 min at room temperature (25 °C) with Fura-4F AM (5 μM) dissolved in DMSO. A final spin and resuspension of mitochondria were performed to remove any residual dye. To measure $[Ca^{2+}]_e$, Fura-4F penta-potassium (1 μM) was added to the respiration buffer. $\Delta\Psi_m$ was measured using the lipophilic dye TMRM (1 μM, Invitrogen™, Eugene, OR) in a ratiometric excitation approach (Scaduto and Grotyohann 1999). NADH was measured by its autofluorescence (Blomeyer et al. 2013; Boelens et al. 2013; Haumann et al. 2010). To ensure identical conditions as for the $[Ca^{2+}]_m$ measurement, mitochondria were incubated with the appropriate concentration of DMSO for 30 min at 25 °C before measuring $[Ca^{2+}]_e$, $\Delta\Psi_m$, and NADH. $[Ca^{2+}]_e$ and $\Delta\Psi_m$ were measured by directly adding the appropriate dye to the respiration buffer.

Measurement of free Ca^{2+}

The Ca^{2+} measurements in this study represent the free matrix and extra-matrix Ca^{2+} for both protocols whereas the added $CaCl_2$ (10–40 μM) represents the total amount of $CaCl_2$ added to the cuvette. The molecular dye Fura-4F was used to measure concentrations of both matrix and extra-matrix free Ca^{2+}. The vendor specified dissociation constant (K_d) of Fura-4F is 770 nM. However, when loaded in mitochondria, we determined a K_d of 890 nM. At an emission wavelength (λ_{em}) of 510 nm, the peak of the excitation wavelength (λ_{ex}) of Fura-4F shifted from 380 nm to 340 nm on binding Ca^{2+} to the dye molecules. Measuring Ca^{2+} at these wavelengths was not influenced by background noise (e.g. NADH autofluorescence), so a background subtraction was unnecessary. For calibration, ratios were obtained when all Fura-4F had become bound to Ca^{2+} (R_{max}) and when no Ca^{2+} was bound to Fura-4F (R_{min}). To determine these ratios, experiments were conducted in PA energized mitochondria using 500 nM CsA, 500 μM $CaCl_2$ for R_{max}, and A23187 (Ca^{2+}-ionophore) in the presence of 2.5 mM EGTA for R_{min}. The $[Ca^{2+}]_m$ was calculated using the following equation (Grynkiewicz et al. 1985):

$$\left[\mathrm{Ca}^{2=}\right]_{\mathrm{m}} = K_d \cdot \frac{S_{f2}}{S_{b2}} \cdot \frac{R - R_{\min}}{R_{\max} - R} \quad (1)$$

K_d is 890 nM, S_{f2} is the signal intensity of free Fura-4F measured at 380 nm, and S_{b2} is the signal intensity of Ca^{2+}-saturated Fura-4F measured at 380 nm. Their values were obtained from the R_{max} and R_{min} experiments, which were done for each preparation. For details, see Supplemental Figs. S1 and S2 for the fluorescence spectra in the presence of various amounts of Ca^{2+} and calibration of Fura-4F, respectively. Calibration of the Fura-4F penta-potassium signal in the presence of mitochondria was slightly different from the one used for Fura-4F AM. R_{min} was measured in respiration buffer with added 100 μM EGTA without added $CaCl_2$ to chelate all the Ca^{2+}, while R_{max} was determined in the respiration buffer containing 1 mM $CaCl_2$. Ca^{2+} fluorescent measurements and calculation of $[Ca^{2+}]_e$ were conducted in the same manner as described above for $[Ca^{2+}]_m$. Free $[Mg^{2+}]$ was not measured in this study. Our previous study showed that the calculated buffer $[Mg^{2+}]$ after adding $MgCl_2$ was nearly identical to the $[Mg^{2+}]$ measured using Mag-Fura-2 fluorescence (Boelens et al. 2013).

Measurement of NADH

NADH autofluorescence signals were measured at λ_{ex} of 350 nm and λ_{em} of 456 nm. For calibration, the NADH pool was either fully oxidized (0 %) with the respiratory uncoupler carbonyl cyanide 3-chlorophenylhydrazone (CCCP, 4 μM), or fully reduced (100 %) with the complex I blocker rotenone (10 μM).

Measurement of $\Delta\Psi_m$

Fluorescence changes using TMRM were detected by two λ_{ex} (546 and 573 nm) and one λ_{em} (590 nm). Using the ratio of the emission at both excitation wavelengths (573/546) has the advantage of a higher dynamic range when compared to a single wavelength technique (Scaduto and Grotyohann 1999). At the end of each protocol at t = 720 s, CCCP (4 μM) was added to fully depolarize mitochondria.

Statistical analyses

The data from four hearts were pooled separately for each of the four fluorescence measurements. Data were transferred from PTI FelixGX (Version 3) into Microsoft® Excel® (2007). IBM® SPSS® (Version 19) was used to execute statistical analysis, which was performed using one-way analysis of variance followed by post hoc Tukey's range test to examine differences among individual groups. Changes were considered statistically significant when the p-value was set at ≤0.05. Data for analyses were collected at the times given below and are presented as means ± SEM. For some analyses, results are presented as means ± standard deviation. Statistical tests were performed to compare changes in $[Ca^{2+}]_m$ averaged from 60 to 70 s of all 30 possible treatment combinations for the five $[CaCl_2]$, three $[MgCl_2]$, and two protocol effects.

Calculation of mitochondrial Ca^{2+} buffering power

Initial rates of Ca^{2+} flux for both the uptake and extrusion phases were derived from the data and converted from $d[Ca^{2+}]_e/dt$ to $d[Ca^{2+}]_{tot}/dt$ using the method outlined in Bazil et al. (2013). Briefly, non-linear trend lines were fitted to the data shown in Figs. 2 and 4, and the analytical derivatives were used to compute the rate of change in free Ca^{2+}. Trend line fits to the extra-matrix and matrix dynamics are shown in Supplemental Figs. S4 and S5, respectively. The extra-matrix rates were converted to total Ca^{2+} flux by using the known buffering power of EGTA. For simplicity, all Ca^{2+} uptake rates were assumed to be through the MCU and all Ca^{2+} release rates were assumed to be via the NCE. To compute the mitochondrial Ca^{2+} buffering power, the approach described in Bazil et al. (2013) was used. Specifically, the buffering power was calculated using the Ca^{2+} extrusion phase of the free Ca^{2+} dynamics profiles. The calculated Ca^{2+} buffering power was expressed as:

$$\beta_{Ca,m}=1+\sum_i \frac{n_i^2\left[Ca^{2+}\right]_m^{n_i-1}\left[B_{Ca,i}\right]_m}{K_{Ca,i}^{n_i}\left(1+\left[Ca^{2+}\right]_m^{n_i}/K_{ca,i}^{n_i}\right)^2} \quad (2)$$

Results

Changes in extra-matrix ionized Ca^{2+}

The dynamics of extra-matrix free Ca^{2+} for each protocol (A and B) and experimental conditions are shown in Fig. 2. Fluorescence ratios were converted to concentrations using Eq. 1. Each panel consists of five different traces representing one concentration of $CaCl_2$ added (0, 10, 20, 30, or 40 μM) at one of three fixed $MgCl_2$ concentrations (0, 0.5, or 1.0 mM) in the presence of 40 μM EGTA. The dynamics of lower $CaCl_2$ concentrations (0, 10, and 20 μM) are illustrated in more detail in the insets that show axes with the same labels seen in the main figure panels. Panels a–c show the Ca^{2+} dynamics profile using Protocol A, whereas panels d–f depict the Ca^{2+} dynamics profile using protocol B.

On a gross scale, the rates of decrease in $[Ca^{2+}]_e$ (Ca^{2+}uptake rates), magnitude of uptake before addition of RR, and the rates of increase in $[Ca^{2+}]_e$ (Ca^{2+} efflux rates) after addition of NaCl, were similar in each protocol for the same $[CaCl_2]$ and $[MgCl_2]$ combination (Fig. 2). And as expected, Ca^{2+} uptake was attenuated when $MgCl_2$ was included in the buffer. However, distinct differences in the rates of Ca^{2+} uptake between each protocol were revealed by careful analysis. Double exponential functions fit to the Ca^{2+} uptake dynamics for protocol A revealed that the overall dynamics consisted of two time scales as shown in Fig. 3. These trend lines were fit between 60 and 150 s of the early phase of the uptake as shown in Supplemental Fig. S4. A single exponential function was sufficient to characterize the Ca^{2+} uptake dynamics for protocol B for all $[CaCl_2]$ and $[MgCl_2]$ combinations except for 40 μM $CaCl_2$ (data not shown). For this concentration of $CaCl_2$, a double exponential function was a better fit with similar time constants for the 40 μM $CaCl_2$ condition in protocol A. For additions of $CaCl_2$ of 10 μM and below, the dynamics of $[Ca^{2+}]_e$ were at or below detectable limits and were not used in the analysis. Furthermore, adding 40 μM $CaCl_2$ in the presence of 0.5 or 1.0 mM $MgCl_2$ in either protocol induced a faster Ca^{2+} uptake rate

compared to 30 μM $CaCl_2$, which resulted in lower levels of $[Ca^{2+}]_e$ before addition of RR and NaCl.

Changes in matrix ionized Ca^{2+}

Using the same protocols (A and B) shown in Fig. 1, $CaCl_2$ was added and $[Ca^{2+}]_m$ was measured. As with the extra-matrix Ca^{2+}, the fluorescent ratios were converted to concentrations using Eq. 1. Fura-4F AM loading and washout was confirmed by ensuring that $[Ca^{2+}]_m$ did not change after adding EGTA to the buffer (not shown). The results are displayed in Fig. 4 with a similar layout of the figure panels (a–f) shown in Fig. 2. Note that a very high $[Ca^{2+}]_m$ was attained because CsA had been added to the buffer in all experiments. Panels a–c and d–f show $[Ca^{2+}]_m$ dynamics at 0, 0.5 and 1.0 mM $MgCl_2$ using protocol A and protocol B, respectively. Matrix free Ca^{2+} dynamics were quantitatively and qualitatively different for each protocol and $CaCl_2/MgCl_2$ combination. For protocol A (Fig. 4, panels a–c), adding $CaCl_2$ (10, 20, 30, or 40 μM) induced an abrupt and rapid uptake of Ca^{2+}. Adding lower $[CaCl_2]$ (10 and 20 μM, see insets) caused smaller increases in peak $[Ca^{2+}]_m$ compared to the higher $[CaCl_2]$ (30 and 40 μM). Nonetheless, even at lower $[CaCl_2]$ (10 and 20 μM), there was an abrupt increase in Ca^{2+} uptake when $CaCl_2$ was added to mitochondria. Note that in protocol A the Ca^{2+} uptake at any $[CaCl_2]$ showed an initial fast Ca^{2+} uptake phase followed by a slower gradual Ca^{2+} uptake phase. This fast uptake was not observed in protocol B.

Figure 5 shows the measured $[Ca^{2+}]_m$ recorded over a few seconds (averaged from 60 to 70 s) for protocols A and B. For the 20 and 30 μM $CaCl_2$ additions across all $MgCl_2$ conditions using protocol A, there were statistically significant differences in $[Ca^{2+}]_m$ when compared to the same $CaCl_2$ and $MgCl_2$ combination using protocol B ($p \leq 0.05$). The presence of added $MgCl_2$ in the respiration buffer attenuated the maximal $[Ca^{2+}]_m$ in a concentration-dependent manner at each $[CaCl_2]$ except for the 40 μM $CaCl_2$. For protocol B (Fig. 4, panels d–f), mitochondrial Ca^{2+} uptake was slower and more gradual at the lower $[CaCl_2]$ (10, 20, and 30 μM) as shown in the insets of Figs. 2 and 4. However, in the 40 μM $CaCl_2$ group, adding mitochondria to respiration buffer with $CaCl_2$ already present (protocol B) showed a similar fast Ca^{2+} uptake rate as observed in protocol A. After adding 40 μM $CaCl_2$ in protocol B, the fluorescent signal was close to R_{max}; thus the calculated $[Ca^{2+}]_m$ was very noisy and likely not representative of the true value of $[Ca^{2+}]_m$. For protocol A and during exposure to low $CaCl_2$ (10–30 μM), the $[Ca^{2+}]_m$ attained during the slow uptake, but not the initial fast uptake phase, was significantly different among the $MgCl_2$ additions for a given $[CaCl_2]$. Overall, a comparison of these protocols shows that there exists a Mg^{2+}-insensitive, fast component of Ca^{2+} uptake that appears only when $CaCl_2$ is added to buffer already containing mitochondria, or when the $[CaCl_2]$ is high enough. The addition of RR (1 μM) completely inhibited Ca^{2+} uptake in both protocols A and B. Furthermore, at 40 μM $CaCl_2$ the similarity in the rate of uptake between the two protocols is a verification to the equivalent rapidity of mixing of substances added to the cuvette.

Changes in $\Delta\Psi_m$ and NADH

In parallel studies, $\Delta\Psi_m$ and NADH were measured to confirm that the differences observed in Ca^{2+} uptake dynamics were not due to changes in bioenergetics. Experimental conditions

were simplified to consist of 0 and 1.0 mM $MgCl_2$ and 0 and 40 μM $CaCl_2$ combinations. Figure 6, panels a and b, and panels c and d, summarize changes in $\Delta\Psi_m$ and NADH, respectively during protocol A and protocol B. Note that the starting point for the two variables in the figure were slightly different, with the start point at 30 and 60 s for protocols A and B, respectively. There were no significant differences observed in either $\Delta\Psi_m$ or NADH between the two protocols. In addition, $\Delta\Psi_m$ and NADH were not significantly affected by adding 40 μM $CaCl_2$ (protocol A and B) in either the presence or absence of 1 mM $MgCl_2$, which indicates that mitochondrial bioenergetics was not affected by the nature of mitochondrial exposure to $CaCl_2$ (protocol A vs. protocol B) or $MgCl_2$.

Mitochondrial Ca^{2+} buffering power

The Ca^{2+} uptake dynamics obtained under protocols A and B that are shown in Figs. 2 and 4 were used to calculate the mitochondrial Ca^{2+} buffering power (βCa^{2+}_m) as a function of $[Ca^{2+}]_m$ using Eq. 2 and shown in Fig. 7. At low $[Ca^{2+}]_m$, βCa^{2+}_m was nearly 3000:1 (total matrix $[Ca^{2+}]$:free matrix $[Ca^{2+}]$) but rose to 10,000:1 as $[Ca^{2+}]_m$ was increased beyond 5 μM. The calculated βCa^{2+}_m values for $[Ca^{2+}]_m$ below 500 nM were highly variable due to the $[Ca^{2+}]_m$ measurement limitations discussed above. When $MgCl_2$ was present, βCa^{2+}_m no longer increased as much and began to decrease as $[Ca^{2+}]_m$ increased further in a concentration-dependent manner. Based on a two component-buffering model for matrix Ca^{2+}, this decrease in βCa^{2+}_m is likely due to an effect of Mg^{2+} to reduce the Ca^{2+} binding capacity for the class 2 buffers. The effect of $[Mg^{2+}]_e$ on the sequestration parameters is summarized in Table 1. Although higher $[Ca^{2+}]_m$ were attained with protocol A due to increased MCU activity triggered by the activation of both fast and slow modes of Ca^{2+} uptake, βCa^{2+}_m was invariant with respect to either protocol A or B and was uniquely set both by $[Ca^{2+}]_m$ and by $[Mg^{2+}]_e$.

Mg^{2+} attenuates both Ca^{2+} uptake and efflux

The data shown in Figs. 2 and 4 were also used to calculate the rates for the slow mode Ca^{2+} uptake by MCU and extrusion by mNCE under the experimental conditions used in this study. Note that these transport rates were calculated using $J_{Ca2+,tot} = (d[Ca^{2+}]m/dt)*\beta_{Ca2+,m}$ within 10 s of $CaCl_2$ or NaCl-induced perturbations. Mg^{2+} was found to attenuate both the slow mode of Ca^{2+} uptake by MCU (Fig. 8a) and the release by mNCE (Fig. 8b). The slow mode Ca^{2+} uptake rates in protocol B were about 40 % of the slow mode Ca^{2+} uptake rates in protocol A for all three extra-matrix $MgCl_2$ levels. The extrusion rates were independent of the Ca^{2+} loading protocol, i.e. protocol A vs. protocol B. These rates were estimated from the $[Ca^{2+}]_e$ dynamics by averaging the rates between 75 and 90 s and 360–390 s for Ca^{2+} uptake and extrusion, respectively.

Discussion

Mitochondrial Ca^{2+} uptake modes

In our examination of factors that affect mitochondrial Ca^{2+} handling (influx, efflux and sequestration), we measured extra-matrix and matrix free Ca^{2+} dynamics in isolated cardiac mitochondria using various combinations of $[CaCl_2]$ and $[MgCl_2]$ under two different Ca^{2+} loading protocols (Fig. 1). The order of addition, i.e. mitochondria before $CaCl_2$ or

mitochondria after $CaCl_2$, resulted in significant differences in mitochondrial Ca^{2+} uptake dynamics. In protocol A, mitochondria displayed a fast Ca^{2+} uptake profile at each [$CaCl_2$] that was followed by a slower and more gradual Ca^{2+} uptake profile when $CaCl_2$ was added first as a bolus and mitochondria after that in the presence or absence of $MgCl_2$. These two modes are evident from the time constant analyses summarized in Fig. 3 and the degree of Ca^{2+} uptake depicted in Fig. 5. In protocol B, when mitochondria were exposed to the buffer containing $CaCl_2$ already present with or without $MgCl_2$, Ca^{2+} uptake was slower and more gradual at $CaCl_2$ concentrations below 40 μM. Therefore, when compared to protocol A, only the slower mode of Ca^{2+} uptake was apparent at the lower [$CaCl_2$] in protocol B. These differences in Ca^{2+} uptake between the two protocols were not due to differences in $\Delta\Psi_m$ as indicated in Fig. 4a, b. This finding is further supported by the data of Supplemental Fig. S3, which shows that in the absence of PA before adding $CaCl_2$ first or mitochondria first, the different uptake modes remained evident as in the original two main protocols in which PA was present. The presence of extra-matrix $MgCl_2$ markedly attenuated the slow, but not the fast, component of Ca^{2+} uptake and altered mitochondrial Ca^{2+} buffering (sequestration) power (Figs. 7 and 8). This is also evident by the decreasing effect of Mg^{2+} on the slow time constants shown in Fig. 3. Also, note that the fast time constants were relatively insensitive to Mg^{2+}, which further supports the Mg^{2+} independent nature of the fast uptake shown in Fig. 5. These two potential modes of Ca^{2+} uptake are consistent with our recent computational modeling report on the dynamics of Ca^{2+} uptake (Tewari et al. 2014). Interestingly, the analysis also revealed that the slow mode was inhibited in protocol B reaching only 40 % of the rate observed during protocol A regardless of $[Mg^{2+}]_e$ as shown in Fig. 8a (compare dashed lines vs. solid lines). We suggest that there are two distinct modes of Ca^{2+} uptake that occur at physiological levels of cytosolic Ca^{2+} and Mg^{2+}. One mode is a fast, Mg^{2+}-insensitive Ca^{2+} uptake pathway that could be modeled as a RyR-type channel (Tewari et al. 2014) and the other is a slower Mg^{2+}-sensitive Ca^{2+} uptake pathway (Pradhan et al. 2011), that is also modulated by the mode of Ca^{2+} delivery. Moreover, the Mg^{2+}-insensitive nature of the fast mode we found in the present study is compatible with the data on Mg^{2+}-insensitive RaM of Ca^{2+} uptake reported by Gunter et al. (1998). Our findings are also consistent with the attenuating effect of Mg^{2+} on the slow mode of Ca^{2+} uptake reported earlier by our group (Boelens et al. 2013).

The focus of this study was not to characterize the regulatory action of the molecular components of the MCU complex; however, it suffices to note that the differences in uptake could be attributed to a differential regulation of MCU during exposure to different $CaCl_2$ with and without $MgCl_2$. It is possible that the marked differences in the two modes of Ca^{2+} uptake we found are attributable to the MCU complex and its regulatory subunits, e.g. MICU1 and MICU2 (Marchi and Pinton 2014; Patron et al. 2014; Mallilankaraman et al. 2012). MICU1 appears to act in response to high cytosolic [Ca^{2+}] by stimulating Ca^{2+} uptake by MCU, whereas MICU2 appears to inhibit MCU functions at a lower cytosolic [Ca^{2+}] (Patron et al. 2014; Kamer and Mootha 2014). However, major controversies abound in these observations, with conflicting results reported (Marchi and Pinton 2014; Patron et al. 2014; Mallilankaraman et al. 2012). Some of the discrepancies might be due to the composition of the buffer. For example, in one report Mg^{2+}, an allosteric modulator of MCU activity was present, whereas in another study it was absent (Csordas et al. 2013;

Mallilankaraman et al. 2012). And while incontrovertible evidence of MCU inhibition by Mg^{2+} exists (see, for example, Kirichok et al. 2004), the molecular components responsible remain unidentified. The ability of the Ca^{2+} delivery method to unmask different modes of MCU activity could be attributed to its effect on the state of the EF-hands located on the MICU1 and/or MICU2 regulatory subunits. For example, if the MICU1 and MICU2 subunits act in conjunction as a Ca^{2+}-sensitive break mechanism (Patron et al. 2014; Kamer and Mootha 2014), a rapid change in Ca^{2+} near the subunits may temporarily release the break and result in a brief, rapid uptake of Ca^{2+}. That said, the present study is focused on the observation of a fast and slow mode of Ca^{2+} uptake that is dependent on the manner by which mitochondria are exposed to a bolus of $CaCl_2$, and not specifically on the regulation by MICU1, MICU2, and other regulatory proteins. Future elaborate studies in the contribution of these proteins to these two modes of Ca^{2+} in the presence and absence of Mg^{2+}, and the impact on the mitochondrial Ca^{2+} buffering capacity should be undertaken.

It is evident that mitochondria took up Ca^{2+} in a quick and robust manner when $CaCl_2$ was added to the mitochondrial suspension (protocol A). In contrast, the matrix free Ca^{2+} dynamics data showed that when mitochondria were added to respiration buffer with $CaCl_2$ already present, the fast uptake mode was abolished for all $CaCl_2$ concentrations except for the highest [$CaCl_2$] (40 μM). Note that the order of adding 40 μM $CaCl_2$ and mitochondria to the respiration buffer resulted in similar Ca^{2+} uptake profile for both protocols. This indicates that the rapid mixing of the cuvette content assured near instantaneous homogenous mixture, and that the difference in Ca^{2+} uptake between the two protocols was mostly due to the different modes of uptake in mitochondria and not to an uneven mix of the added $CaCl_2$. The order of adding mitochondria or $CaCl_2$ also did not affect the $\Delta\Psi$ or redox state indicating that mitochondria were fully energized in the presence of PA when mitochondria were added before or after adding $CaCl_2$. These observations provide further evidence that the method of exposure to Ca^{2+}, and not bioenergetic differences such as $\Delta\Psi$, is the regulatory mechanism behind the vastly different uptake modes observed in our study. In addition, this difference in Ca^{2+} uptake was more apparent when $MgCl_2$ was included in the respiration buffer of either Ca^{2+} loading protocol. This difference in the mode of Ca^{2+} uptake was also not dependent on the mitochondrial redox state because the NADH autofluorescence data (Fig. 6) showed no observable difference between the two protocols (A and B), in the presence or absence of added $CaCl_2$ or $MgCl_2$.

Based on these observations, we can conclude that Mg^{2+} regulates bulk Ca^{2+} uptake by attenuating mainly the slow component of the MCU-mediated Ca^{2+} uptake in a concentration-dependent manner. This conclusion is supported by our previous findings (Boelens et al. 2013) and recent computational models (Tewari et al. 2014; Bazil and Dash 2011) and indicates that the MCU is capable of operating in multiple conductance modes. In addition, the data revealed another intriguing aspect of the Ca^{2+}-dependent regulation of mitochondrial Ca^{2+} uptake. As shown in Fig. 2, the 40 μM $CaCl_2$ bolus resulted in a lower $[Ca^{2+}]_e$ at the time of RR addition compared to the 30 μM $CaCl_2$ bolus for either protocol. In other words, a higher bolus of $CaCl_2$ resulted in more Ca^{2+} being taken up by mitochondria, which was inhibited by Mg^{2+} in a concentration-dependent manner. We speculate that this phenomenon is due to differential regulation or modulation of MCU

conductance/open probability times by other components of the protein complex (e.g. MICU1 and MICU2) (Kamer and Mootha 2014; Harrington and Murphy 2015).

The Mg^{2+}-sensitivity of the MCU complex likely plays a role in heart failure, ischemia and reperfusion injury, and other related events in the myocardium (for review see Douban et al. 1996; Kolte et al. 2014; Levitsky and Takahashi 2013). For example, cytosolic [Mg^{2+}] is known to rise during ischemia due to net ATP hydrolysis. This rise in [Mg^{2+}] would help mitigate mitochondrial Ca^{2+} loading via MCU, but the Ca^{2+} buffering system would be compromised, which could counter the Mg^{2+} effect and contribute to mitochondrial Ca^{2+} overload. In heart failure, the net decrease in cellular Mg^{2+} content would lead to more mitochondrial Ca^{2+} uptake via the MCU. Based on our results reported herein, the decrease in cytosolic [Mg^{2+}] levels observed in these pathophysiological conditions, e.g. heart failure, would likely result in elevated $[Ca^{2+}]_m$. This would likely induce Ca^{2+}-mediated mitochondrial dysfunction, and if the local cytosolic [Ca^{2+}] is high, also possibly trigger mPTP opening with concomitant cell death. Indeed, it has been reported that the cardiovascular consequences of Mg^{2+} deficiency in clinical studies include multifocal necrosis with Ca^{2+} accumulation in mitochondria in a pattern suggestive of myocardial infarction (Seelig 1989).

$MgCl_2$ and mitochondrial mNCE-induced Ca^{2+} efflux

The well-known effect of Mg^{2+} to attenuate Ca^{2+} uptake and its extrusion is demonstrated in greater detail by our data. The rate of increase in $[Ca^{2+}]_m$ significantly decreased as a function of $[Mg^{2+}]_e$ with an apparent K_i of 0.25 mM (Fig. 8a). This value is similar to that of our previously determined computational model of Ca^{2+} uptake (Pradhan et al. 2011). At 1 mM $[Mg^{2+}]_e$, close to the physiological extra-matrix level, the MCU complex was inhibited by greater than 15-fold at the peak of a 1 μM cytosolic Ca^{2+} transient. Despite this, $[Ca^{2+}]_m$ reached close to 1 μM with addition of 20 μM $CaCl_2$ (Fig. 4c) due to the rapid uptake mode by the MCU complex. Incidentally, $[Mg^{2+}]_e$ also inhibits Na^+-dependent Ca^{2+} efflux (Wingrove and Gunter 1986), which is consistent with some of our current findings (Fig. 8b). Here, it is shown that Mg^{2+} with a K_i of 1 mM inhibited the rate of decrease in $[Ca^{2+}]_m$. Moreover, the maximal rate of Ca^{2+} efflux was reduced to half when $[Mg^{2+}]_e$ was increased from 0 mM to 1 mM. So not only is Ca^{2+} uptake slowed when there is an increase in $[Mg^{2+}]_e$, but also the rate of Ca^{2+} extrusion is impeded. Whereas it appears to be clear that $[Mg^{2+}]_e$ regulates the slower phase of Ca^{2+} uptake, the Mg^{2+}-insensitive rapid component of the MCU complex can lead to net Ca^{2+} uptake when mitochondria are presented with sufficiently high, pulse-like Ca^{2+} transients.

Mitochondrial Ca^{2+} buffering

The data from this study also corroborates previous reports that the mitochondrial Ca^{2+} sequestration system consists of at least two classes of buffers (Wei et al. 2012; Bazil et al. 2013; Blomeyer et al. 2013) (Fig. 7) and challenges recent findings (Wei et al. 2012; Tewari et al. 2014) that suggest the manner in which Ca^{2+} is loaded into mitochondria (fast vs. slow) modulates the degree of Ca^{2+} buffering. In our prior study, we used indo-1 to monitor [Ca^{2+}] in both the extra-matrix and matrix compartments and mitochondrial Ca^{2+} buffering (Blomeyer et al. 2013). In contrast, in the current study we used Fura-4F because it can

register higher [Ca^{2+}] than indo-1 without saturating. Consequently, we also added CsA to the experimental buffer to prevent mPTP opening induced by high $[Ca^{2+}]_m$. As a result of using a different Ca^{2+} indicator dye and different experimental conditions, we observed somewhat different buffering parameters between the current and previous studies (Bazil et al. 2013; Blomeyer et al. 2013) that can be explained by the different extent of dye loading, cation binding properties between each type of Ca^{2+} fluorescence dye, and experimental conditions. Despite these differences, the general properties of the sequestration system identified in this study are identical to our previous reports (Bazil et al. 2013; Blomeyer et al. 2013). That is, the class 1 buffers are of the prototypical type and consist of binding sites that bind a single Ca^{2+} ion, whereas the class 2 buffers are capable of binding multiple Ca^{2+} ions at a single site in a cooperative fashion.

There is strong supporting evidence that the class 2 buffers consist of complexes formed by the annexin class of proteins in conjunction with acidic phospholipids in the membrane that promote or facilitate the formation of CaPi granules on the inner leaflets of the inner mitochondrial membrane (IMM) (for discussion, see Bazil et al. 2013). In our present study, we show that Mg^{2+} also modulates this class of Ca^{2+} buffers but does not regulate the class 1 buffers (Fig. 7). The mechanisms by which Mg^{2+} alters Ca^{2+} sequestration is unclear but may involve two mechanisms: i) extra-mitochondrial Mg^{2+} alters the class 2 buffer affinity for Ca^{2+} or ii) matrix Mg^{2+} encumbers the formation of CaPi complexes in the matrix on the surface of the IMM. We propose that latter is more likely. Based on earlier reports by Brierley et al. (1962, 1963, 1964), Mg^{2+} is actively loaded into energized mitochondria in a Pi-dependent and -independent manner. Therefore, Pi levels might modulate Mg^{2+} uptake during Ca^{2+} loading which would result in an increase in matrix Mg^{2+} content. However, Boelens et al. (2013) reported that increasing buffer $MgCl_2$ did not change $[Mg^{2+}]_m$ appreciably over time. In that study, Ca^{2+} uptake was absent, and the internal mechanisms regulating matrix Mg^{2+} were already in homeostasis. A plausible hypothesis is that Mg^{2+} enters mitochondria concomitantly with Ca^{2+} and interferes with CaPi granule formation. This is consistent with the observation that Mg^{2+} prevents and slows the spontaneous transition of CaPi from an amorphous state to a crystalline state (Wu et al. 2008, 2009). Nevertheless, our results demonstrate that when $[Mg^{2+}]_e$ is elevated, the ability of mitochondria to sequester large amounts of Ca^{2+} is hindered.

Summary and perspective

The mechanism by which isolated mitochondria take up and sequester Ca^{2+} is a complex function not only of how much Ca^{2+} mitochondria are exposed to, but also the experimental conditions. In one scenario, when added $CaCl_2$ exceeds a threshold, a rapid, Mg^{2+}-insensitive mode of Ca^{2+} uptake is activated. In another scenario, when mitochondria are added to the buffer with low concentrations of EGTA and $CaCl_2$ already present, the rapid mode of Ca^{2+} uptake is not activated, that is unless the buffer concentration of $CaCl_2$ is sufficiently high. Thus, the MCU appears to consist of multiple conductance modes, which are differentially modulated by extra-matrix Mg^{2+}.

Mitochondrial Ca^{2+} homeostasis plays important roles in cellular physiology, regulation of cellular bioenergetics, reactive oxygen species signaling and Ca^{2+} signaling. Agonist-

induced intracellular Ca^{2+} signals can be rapidly transduced to the matrix because mitochondria can exist in close apposition to sites of Ca^{2+} release where local cytosolic [Ca^{2+}] can be higher than in the rest of the cytoplasm (Mallilankaraman et al. 2012). The physiological implications of the different modes of Ca^{2+} uptake in this study are unclear but allude to a process whereby mitochondria can rapidly accumulate and sequester Ca^{2+} to prevent catastrophic cytosolic Ca^{2+} overload, mPTP opening and cell death. Therefore, a better understanding of the Ca^{2+} dynamics and how it is modulated by physiological [Mg^{2+}] could provide new insights into the potential molecular mechanisms that regulate Ca^{2+} fluxes in and out of mitochondria under both physiological and pathophysiological conditions.

Supplementary Material

Refer to Web version on PubMed Central for supplementary material.

Acknowledgments

This work was funded by NIH grants R01-HL095122, P01-GM066730, and K99-HL121160.

References

Agarwal B, Camara AK, Stowe DF, Bosnjak ZJ, Dash RK. Enhanced charge-independent mitochondrial free Ca(2+) and attenuated ADP-induced NADH oxidation by isoflurane: implications for cardioprotection. Biochim Biophys Acta. 2012; 1817(3):453–465. DOI: 10.1016/j.bbabio.2011.11.011 [PubMed: 22155157]

Agarwal B, Dash RK, Stowe DF, Bosnjak ZJ, Camara AK. Isoflurane modulates cardiac mitochondrial bioenergetics by selectively attenuating respiratory complexes. Biochim Biophys Acta. 2014; 1837(3):354–365. DOI: 10.1016/j.bbabio.2013.11.006 [PubMed: 24355434]

Aldakkak M, Camara AK, Heisner JS, Yang M, Stowe DF. Ranolazine reduces Ca^{2+} overload and oxidative stress and improves mitochondrial integrity to protect against ischemia reperfusion injury in isolated hearts. Pharmacol Res. 2011; 64(4):381–392. DOI: 10.1016/j.phrs.2011.06.018 [PubMed: 21741479]

Aldakkak M, Stowe DF, Dash RK, Camara AK. Mitochondrial handling of excess Ca^{2+} is substrate-dependent with implications for reactive oxygen species generation. Free Radic Biol Med. 2013; 56:193–203. DOI: 10.1016/j.freeradbiomed.2012.09.020 [PubMed: 23010495]

An J, Varadarajan SG, Camara A, Chen Q, Novalija E, Gross GJ, et al. Blocking Na(+)/H(+) exchange reduces [Na(+)](i) and [Ca(2+)](i) load after ischemia and improves function in intact hearts. Am J Physiol Heart Circ Physiol. 2001a; 281(6):H2398–H2409. [PubMed: 11709405]

An J, Varadarajan SG, Novalija E, Stowe DF. Ischemic and anesthetic preconditioning reduces cytosolic [Ca^{2+}] and improves Ca(2+) responses in intact hearts. Am J Physiol Heart Circ Physiol. 2001b; 281(4):H1508–H1523. [PubMed: 11557539]

Baughman JM, Perocchi F, Girgis HS, Plovanich M, Belcher-Timme CA, Sancak Y, et al. Integrative genomics identifies MCU as an essential component of the mitochondrial calcium uniporter. Nature. 2011; 476(7360):341–345. DOI: 10.1038/nature10234 [PubMed: 21685886]

Bazil JN, Dash RK. A minimal model for the mitochondrial rapid mode of Ca^{2+} uptake mechanism. PLoS One. 2011; 6(6):e21324.doi: 10.1371/journal.pone.0021324 [PubMed: 21731705]

Bazil JN, Blomeyer CA, Pradhan RK, Camara AK, Dash RK. Modeling the calcium sequestration system in isolated guinea pig cardiac mitochondria. J Bioenerg Biomembr. 2013; 45(3):177–188. DOI: 10.1007/s10863-012-9488-2 [PubMed: 23180139]

Beutner G, Sharma VK, Giovannucci DR, Yule DI, Sheu SS. Identification of a ryanodine receptor in rat heart mitochondria. J Biol Chem. 2001; 276(24):21482–21488. DOI: 10.1074/jbc.M101486200 [PubMed: 11297554]

Blomeyer CA, Bazil JN, Stowe DF, Pradhan RK, Dash RK, Camara AK. Dynamic buffering of mitochondrial Ca^{2+} during Ca^{2+} uptake and Na^{+}-induced Ca^{2+} release. J Bioenerg Biomembr. 2013; 45(3):189–202. DOI: 10.1007/s10863-012-9483-7 [PubMed: 23225099]

Boelens AD, Pradhan RK, Blomeyer CA, Camara AK, Dash RK, Stowe DF. Extra-matrix Mg^{2+} limits Ca^{2+} uptake and modulates Ca^{2+} uptake-independent respiration and redox state in cardiac isolated mitochondria. J Bioenerg Biomembr. 2013; 45(3):203–218. DOI: 10.1007/s10863-013-9500-5 [PubMed: 23456198]

Boyman L, Williams GS, Khananshvili D, Sekler I, Lederer WJ. NCLX: the mitochondrial sodium calcium exchanger. J Mol Cell Cardiol. 2013; 59:205–213. DOI: 10.1016/j.yjmcc.2013.03.012 [PubMed: 23538132]

Boyman L, Chikando AC, Williams GS, Khairallah RJ, Kettlewell S, Ward CW, et al. Calcium movement in cardiac mitochondria. Biophys J. 2014; 107(6):1289–1301. DOI: 10.1016/j.bpj.2014.07.045 [PubMed: 25229137]

Bradford MM. A rapid and sensitive method for the quantitation of microgram quantities of protein utilizing the principle of protein-dye binding. Anal Biochem. 1976; 72:248–254. [PubMed: 942051]

Brierley GP, Bachmann E, Green DE. Active transport of inorganic phosphate and magnesium ions by beef heart mitochondria. Proc Natl Acad Sci U S A. 1962; 48:1928–1935. [PubMed: 14015424]

Brierley G, Murer E, Bachmann E, Green DE. Studies on ion transport. II. The accumulation of inorganic phosphate and magnesium ions by heart mitochondria. J Biol Chem. 1963; 238:3482–3489. [PubMed: 14085406]

Brierley GP, Murer E, O'Brien RL. Studies on ion transport. Vi. The accumulation of Mg^{2+} by heart mitochondria in the absence of inorganic phosphate. Biochim Biophys Acta. 1964; 88:645–647. [PubMed: 14252671]

Buntinas L, Gunter KK, Sparagna GC, Gunter TE. The rapid mode of calcium uptake into heart mitochondria (RaM): comparison to RaM in liver mitochondria. Biochim Biophys Acta. 2001; 1504(2–3):248–261. [PubMed: 11245789]

Cai X, Lytton J. Molecular cloning of a sixth member of the K^{+}-dependent Na^{+}/Ca^{2+} exchanger gene family, NCKX6. J Biol Chem. 2004; 279(7):5867–5876. DOI: 10.1074/jbc.M310908200 [PubMed: 14625281]

Carafoli E. The fateful encounter of mitochondria with calcium: how did it happen? Biochim Biophys Acta. 2010; 1797(6–7):595–606. DOI: 10.1016/j.bbabio.2010.03.024 [PubMed: 20385096]

Chalmers S, Nicholls DG. The relationship between free and total calcium concentrations in the matrix of liver and brain mitochondria. J Biol Chem. 2003; 278(21):19062–19070. DOI: 10.1074/jbc.M212661200 [PubMed: 12660243]

Csordas G, Golenar T, Seifert EL, Kamer KJ, Sancak Y, Perocchi F, et al. MICU1 controls both the threshold and cooperative activation of the mitochondrial Ca(2)(+) uniporter. Cell Metab. 2013; 17(6):976–987. DOI: 10.1016/j.cmet.2013.04.020 [PubMed: 23747253]

De Stefani D, Raffaello A, Teardo E, Szabo I, Rizzuto R. A forty-kilodalton protein of the inner membrane is the mitochondrial calcium uniporter. Nature. 2011; 476(7360):336–340. DOI: 10.1038/nature10230 [PubMed: 21685888]

Dedkova EN, Blatter LA. Calcium signaling in cardiac mitochondria. J Mol Cell Cardiol. 2013; 58:125–133. DOI: 10.1016/j.yjmcc.2012.12.021 [PubMed: 23306007]

Dorn GW 2nd, Maack C. SR and mitochondria: calcium cross-talk between kissing cousins. J Mol Cell Cardiol. 2013; 55:42–49. DOI: 10.1016/j.yjmcc.2012.07.015 [PubMed: 22902320]

Douban S, Brodsky MA, Whang DD, Whang R. Significance of magnesium in congestive heart failure. Am Heart J. 1996; 132(3):664–671. [PubMed: 8800040]

Greenawalt JW, Rossi CS, Lehninger AL. Effect of active accumulation of calcium and phosphate ions on the structure of rat liver mitochondria. J Cell Biol. 1964; 23:21–38. [PubMed: 14228516]

Grynkiewicz G, Poenie M, Tsien RY. A new generation of Ca^{2+} indicators with greatly improved fluorescence properties. J Biol Chem. 1985; 260(6):3440–3450. [PubMed: 3838314]

Gunter TE, Buntinas L, Sparagna GC, Gunter KK. The Ca^{2+} transport mechanisms of mitochondria and Ca^{2+} uptake from physiological-type Ca^{2+} transients. Biochim Biophys Acta. 1998; 1366(1–2):5–15. [PubMed: 9714709]

Harrington JL, Murphy E. The mitochondrial calcium uniporter: mice can live and die without it. J Mol Cell Cardiol. 2015; 78:46–53. DOI: 10.1016/j.yjmcc.2014.10.013 [PubMed: 25451167]

Haumann J, Dash RK, Stowe DF, Boelens AD, Beard DA, Camara AK. Mitochondrial free [Ca^{2+}] increases during ATP/ADP antiport and ADP phosphorylation: exploration of mechanisms. Biophys J. 2010; 99(4):997–1006. DOI: 10.1016/j.bpj.2010.04.069 [PubMed: 20712982]

Huser J, Blatter LA, Sheu SS. Mitochondrial calcium in heart cells: beat-to-beat oscillations or slow integration of cytosolic transients? J Bioenerg Biomembr. 2000; 32(1):27–33. [PubMed: 11768759]

Kamer KJ, Mootha VK. MICU1 and MICU2 play nonredundant roles in the regulation of the mitochondrial calcium uniporter. EMBO Rep. 2014; 15(3):299–307. DOI: 10.1002/embr.201337946 [PubMed: 24503055]

Kirichok Y, Krapivinsky G, Clapham DE. The mitochondrial calcium uniporter is a highly selective ion channel. Nature. 2004; 427(6972):360–364. DOI: 10.1038/nature02246 [PubMed: 14737170]

Kolte D, Vijayaraghavan K, Khera S, Sica DA, Frishman WH. Role of magnesium in cardiovascular diseases. Cardiol Rev. 2014; 22(4):182–192. DOI: 10.1097/CRD.0000000000000003 [PubMed: 24896250]

Kristian T, Pivovarova NB, Fiskum G, Andrews SB. Calcium-induced precipitate formation in brain mitochondria: composition, calcium capacity, and retention. J Neurochem. 2007; 102(4):1346–1356. DOI: 10.1111/j.1471-4159.2007.04626.x [PubMed: 17663756]

Kwong JQ, Lu X, Correll RN, Schwanekamp JA, Vagnozzi RJ, Sargent MA, et al. The mitochondrial calcium uniporter selectively matches metabolic output to acute contractile stress in the heart. Cell Rep. 2015; 12(1):15–22. DOI: 10.1016/j.celrep.2015.06.002 [PubMed: 26119742]

Levitsky DO, Takahashi M. Interplay of Ca(2+) and Mg (2+) in sodium-calcium exchanger and in other Ca(2+)-binding proteins: magnesium, watchdog that blocks each turn if able. Adv Exp Med Biol. 2013; 961:65–78. DOI: 10.1007/978-1-4614-4756-6_7 [PubMed: 23224871]

Lu X, Ginsburg KS, Kettlewell S, Bossuyt J, Smith GL, Bers DM. Measuring local gradients of intramitochondrial [Ca(2+)] in cardiac myocytes during sarcoplasmic reticulum Ca(2+) release. Circ Res. 2013; 112(3):424–431. DOI: 10.1161/CIRCRESAHA.111.300501 [PubMed: 23243207]

Luongo TS, Lambert JP, Yuan A, Zhang X, Gross P, Song J, et al. The mitochondrial calcium uniporter matches energetic supply with cardiac workload during stress and modulates permeability transition. Cell Rep. 2015; 12(1):23–34. DOI: 10.1016/j.celrep.2015.06.017 [PubMed: 26119731]

Mallilankaraman K, Doonan P, Cardenas C, Chandramoorthy HC, Muller M, Miller R, et al. MICU1 is an essential gatekeeper for MCU-mediated mitochondrial Ca(2+) uptake that regulates cell survival. Cell. 2012; 151(3):630–644. DOI: 10.1016/j.cell.2012.10.011 [PubMed: 23101630]

Marchi S, Pinton P. The mitochondrial calcium uniporter complex: molecular components, structure and physiopathological implications. J Physiol. 2014; 592(Pt 5):829–839. DOI: 10.1113/jphysiol.2013.268235 [PubMed: 24366263]

Nicholls DG. Mitochondria and calcium signaling. Cell Calcium. 2005; 38(3–4):311–317. DOI: 10.1016/j.ceca.2005.06.011 [PubMed: 16087232]

O'Rourke B, Blatter LA. Mitochondrial Ca^{2+} uptake: tortoise or hare? J Mol Cell Cardiol. 2009; 46(6):767–774. DOI: 10.1016/j.yjmcc.2008.12.011 [PubMed: 19162034]

Palty R, Ohana E, Hershfinkel M, Volokita M, Elgazar V, Beharier O, et al. Lithium-calcium exchange is mediated by a distinct potassium-independent sodium-calcium exchanger. J Biol Chem. 2004; 279(24):25234–25240. DOI: 10.1074/jbc.M401229200 [PubMed: 15060069]

Pan X, Liu J, Nguyen T, Liu C, Sun J, Teng Y, et al. The physiological role of mitochondrial calcium revealed by mice lacking the mitochondrial calcium uniporter. Nat Cell Biol. 2013; 15(12):1464–1472. DOI: 10.1038/ncb2868 [PubMed: 24212091]

Patron M, Checchetto V, Raffaello A, Teardo E, Vecellio Reane D, Mantoan M, et al. MICU1 and MICU2 finely tune the mitochondrial Ca^{2+} uniporter by exerting opposite effects on MCU activity. Mol Cell. 2014; 53(5):726–737. DOI: 10.1016/j.molcel.2014.01.013 [PubMed: 24560927]

Pradhan RK, Qi F, Beard DA, Dash RK. Characterization of Mg^{2+} inhibition of mitochondrial Ca^{2+} uptake by a mechanistic model of mitochondrial Ca^{2+} uniporter. Biophys J. 2011; 101(9):2071–2081. DOI: 10.1016/j.bpj.2011.09.029 [PubMed: 22067144]

Rasola A, Bernardi P. Mitochondrial permeability transition in Ca(2+)-dependent apoptosis and necrosis. Cell Calcium. 2011; 50(3):222–233. DOI: 10.1016/j.ceca.2011.04.007 [PubMed: 21601280]

Rhodes SS, Ropella KM, Audi SH, Camara AK, Kevin LG, Pagel PS, et al. Cross-bridge kinetics modeled from myoplasmic [Ca^{2+}] and LV pressure at 17 degrees C and after 37 degrees C and 17 degrees C ischemia. Am J Physiol Heart Circ Physiol. 2003; 284(4):H1217–H1229. DOI: 10.1152/ajpheart.00816.2002 [PubMed: 12531735]

Sareen D, Darjatmoko SR, Albert DM, Polans AS. Mitochondria, calcium, and calpain are key mediators of resveratrol-induced apoptosis in breast cancer. Mol Pharmacol. 2007; 72(6):1466–1475. DOI: 10.1124/mol.107.039040 [PubMed: 17848600]

Scaduto RC J, Grotyohann LW. Measurement of mitochondrial membrane potential using fluorescent rhodamine derivatives. Biophys J. 1999; 76(1 Pt 1):469–477. DOI: 10.1016/S0006-3495(99)77214-0 [PubMed: 9876159]

Sedova M, Dedkova EN, Blatter LA. Integration of rapid cytosolic Ca^{2+} signals by mitochondria in cat ventricular myocytes. Am J Physiol Cell Physiol. 2006; 291(5):C840–C850. DOI: 10.1152/ajpcell.00619.2005 [PubMed: 16723510]

Seelig M. Cardiovascular consequences of magnesium deficiency and loss: pathogenesis, prevalence and manifestations–magnesium and chloride loss in refractory potassium repletion. Am J Cardiol. 1989; 63(14):4G–21G.

Sparagna GC, Gunter KK, Sheu SS, Gunter TE. Mitochondrial calcium uptake from physiological-type pulses of calcium. A description of the rapid uptake mode. J Biol Chem. 1995; 270(46):27510–27515. [PubMed: 7499209]

Szabadkai G, Duchen MR. Mitochondria: the hub of cellular Ca^{2+} signaling. Physiology (Bethesda). 2008; 23:84–94. DOI: 10.1152/physiol.00046.2007 [PubMed: 18400691]

Tarasov AI, Griffiths EJ, Rutter GA. Regulation of ATP production by mitochondrial Ca(2+). Cell Calcium. 2012; 52(1):28–35. DOI: 10.1016/j.ceca.2012.03.003 [PubMed: 22502861]

Tewari SG, Camara AK, Stowe DF, Dash RK. Computational analysis of Ca^{2+} dynamics in isolated cardiac mitochondria predicts two distinct modes of Ca^{2+} uptake. J Physiol. 2014; 592(Pt 9):1917–1930. DOI: 10.1113/jphysiol.2013.268847 [PubMed: 24591571]

Thomas RS, Greenawalt JW. Microincineration, electron microscopy, and electron diffraction of calcium phosphate-loaded mitochondria. J Cell Biol. 1968; 39(1):55–76. [PubMed: 4878171]

Varadarajan SG, An J, Novalija E, Smart SC, Stowe DF. Changes in [Na(+)](i), compartmental [Ca(2+)], and NADH with dysfunction after global ischemia in intact hearts. Am J Physiol Heart Circ Physiol. 2001; 280(1):H280–H293. [PubMed: 11123243]

Vasington FD, Murphy JV. Ca^{2+} ion uptake by rat kidney mitochondria and its dependence on respiration and phosphorylation. J Biol Chem. 1962; 237:2670–2677. [PubMed: 13925019]

Wei AC, Liu T, Winslow RL, O'Rourke B. Dynamics of matrix-free Ca^{2+} in cardiac mitochondria: two components of Ca^{2+} uptake and role of phosphate buffering. J Gen Physiol. 2012; 139(6):465–478. DOI: 10.1085/jgp.201210784 [PubMed: 22641641]

Wingrove DE, Gunter TE. Kinetics of mitochondrial calcium transport. II. A kinetic description of the sodium-dependent calcium efflux mechanism of liver mitochondria and inhibition by ruthenium red and by tetraphenylphosphonium. J Biol Chem. 1986; 261(32):15166–15171. [PubMed: 2429966]

Wu LN, Genge BR, Wuthier RE. Analysis and molecular modeling of the formation, structure, and activity of the phosphatidylserine-calcium-phosphate complex associated with biomineralization. J Biol Chem. 2008; 283(7):3827–3838. DOI: 10.1074/jbc.M707653200 [PubMed: 18077457]

Wu LN, Genge BR, Wuthier RE. Differential effects of zinc and magnesium ions on mineralization activity of phosphatidylserine calcium phosphate complexes. J Inorg Biochem. 2009; 103(7):948–962. DOI: 10.1016/j.jinorgbio.2009.04.004 [PubMed: 19477528]

Wu Y, Rasmussen TP, Koval OM, Joiner ML, Hall DD, Chen B, et al. The mitochondrial uniporter controls fight or flight heart rate increases. Nat Commun. 2015; 6:6081.doi: 10.1038/ncomms7081 [PubMed: 25603276]

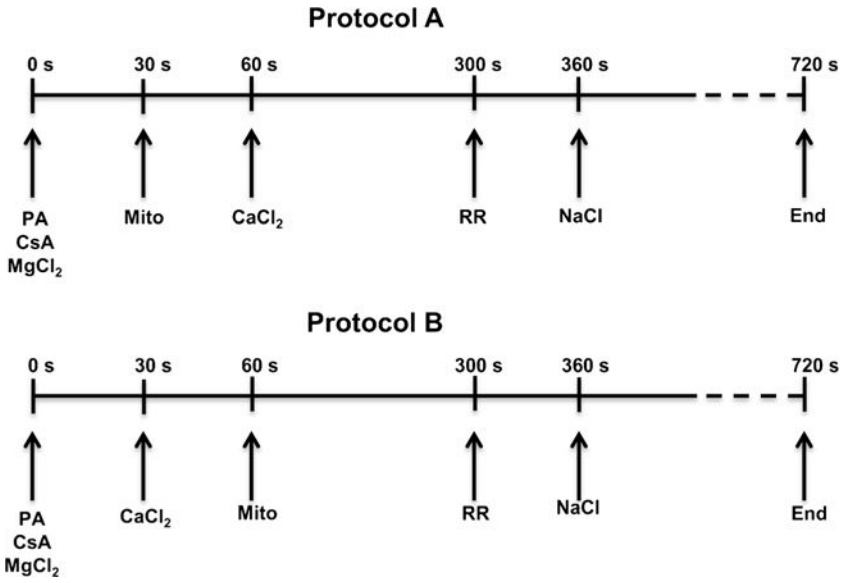

Fig. 1.

Timelines show the two experimental protocols used to characterize and quantify mitochondrial Ca^{2+} handling (influx, efflux, sequestration) in isolated guinea pig cardiac mitochondria. In protocol A, mitochondria were added to the experimental buffer before $CaCl_2$ was added. In protocol B, mitochondria were added to respiration buffer with $CaCl_2$ already present. All other additions were identical between protocols. 40 μM EGTA was present in all the experimental buffers; 0.5 μM CsA was added to all mitochondrial suspensions. Inset axes are the same as the main figure panels

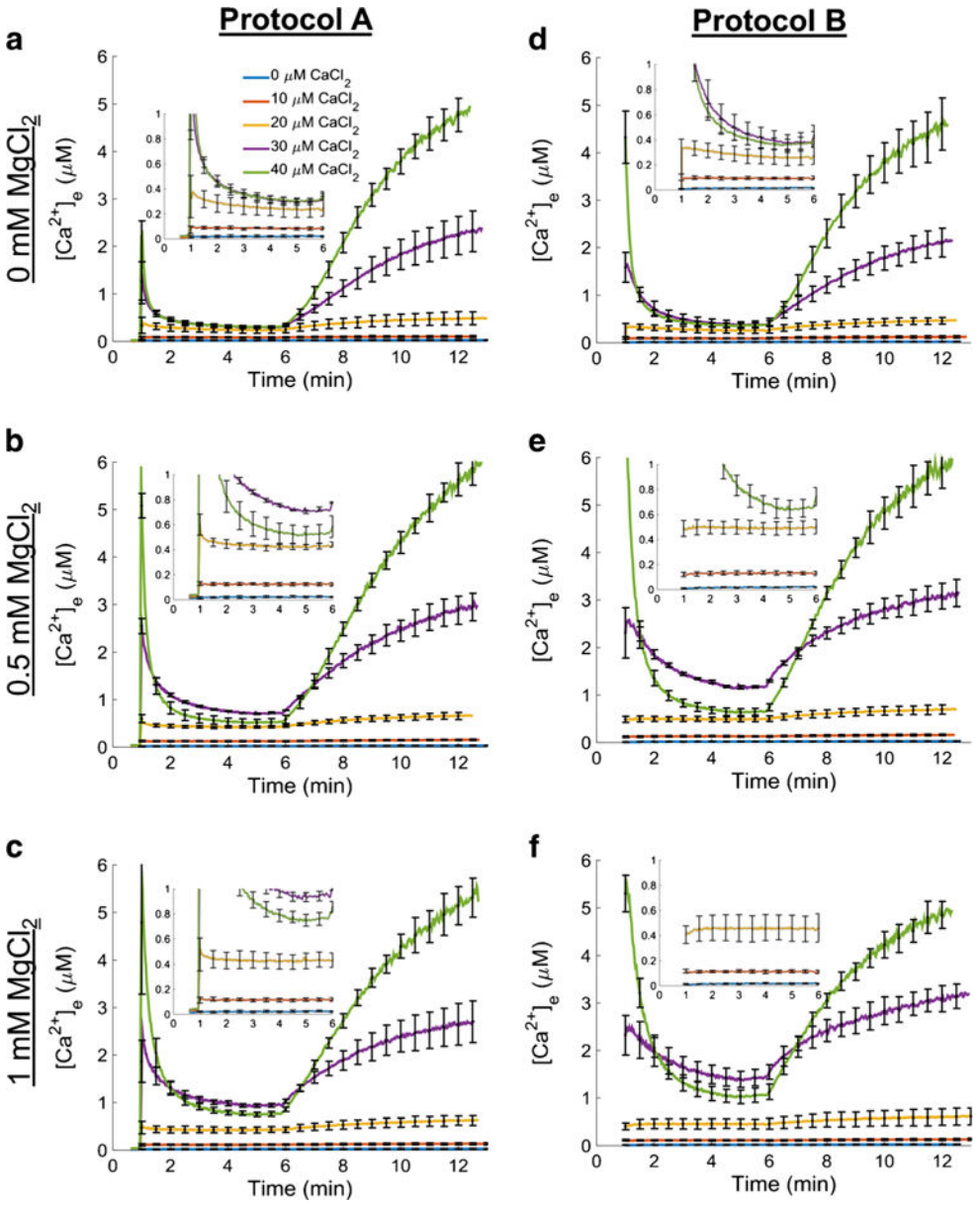

Fig. 2.

Extra-matrix free Ca^{2+} ($[Ca^{2+}]_e$) dynamics. Ca^{2+} uptake and Ca^{2+} release for each combination of $CaCl_2$ and $MgCl_2$ concentrations are shown using the protocol depicted in Fig. 1. $CaCl_2$ was added to respiring mitochondrial suspension (left column; protocol A) or mitochondria were added to the buffer containing a given $CaCl_2$ concentration (right column; protocol B) at 60 s followed by ruthenium red (RR) at 300 s and NaCl at 360 s. The results for protocol A are shown in the left column and the results for protocol B are shown in the right column. Each row corresponds to the buffer $MgCl_2$ indicated on the left of each row. Insets show $[Ca^{2+}]_e$ dynamics for 0, 10, and 20 μM $CaCl_2$ in more detail. The axes are the same as the axes in the main figure panels. Error bars signify standard error of the mean

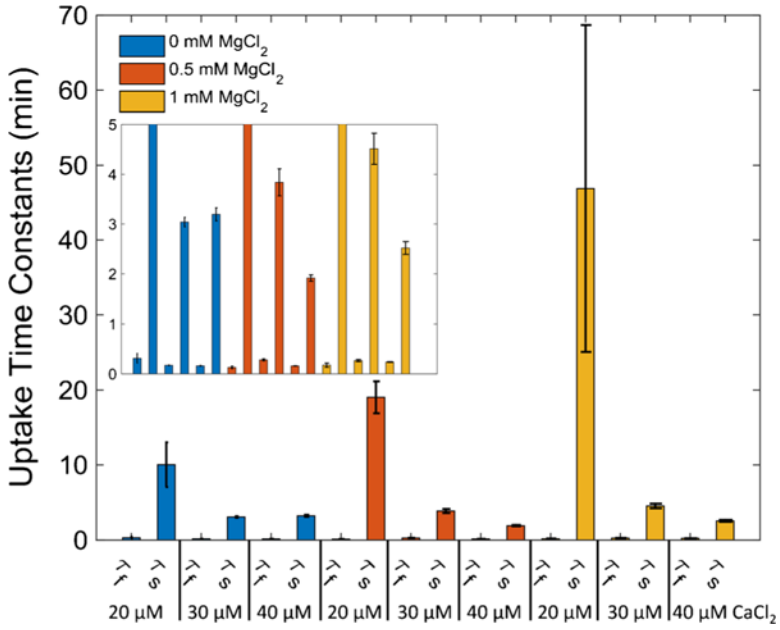

Fig. 3.

Two modes of Ca^{2+} uptake. For $CaCl_2$ concentrations of 20 μM and greater, a double exponential function was fit between 65 s and 150 s to the $[Ca^{2+}]_e$ dynamics observed in protocol A (Fig. 2). The fit time constants show that there was a fast and slow component of Ca^{2+} uptake associated with each bolus of $CaCl_2$ administered. The inset axes labels are the same as the main figure panel. Error bars signify propagated standard deviations

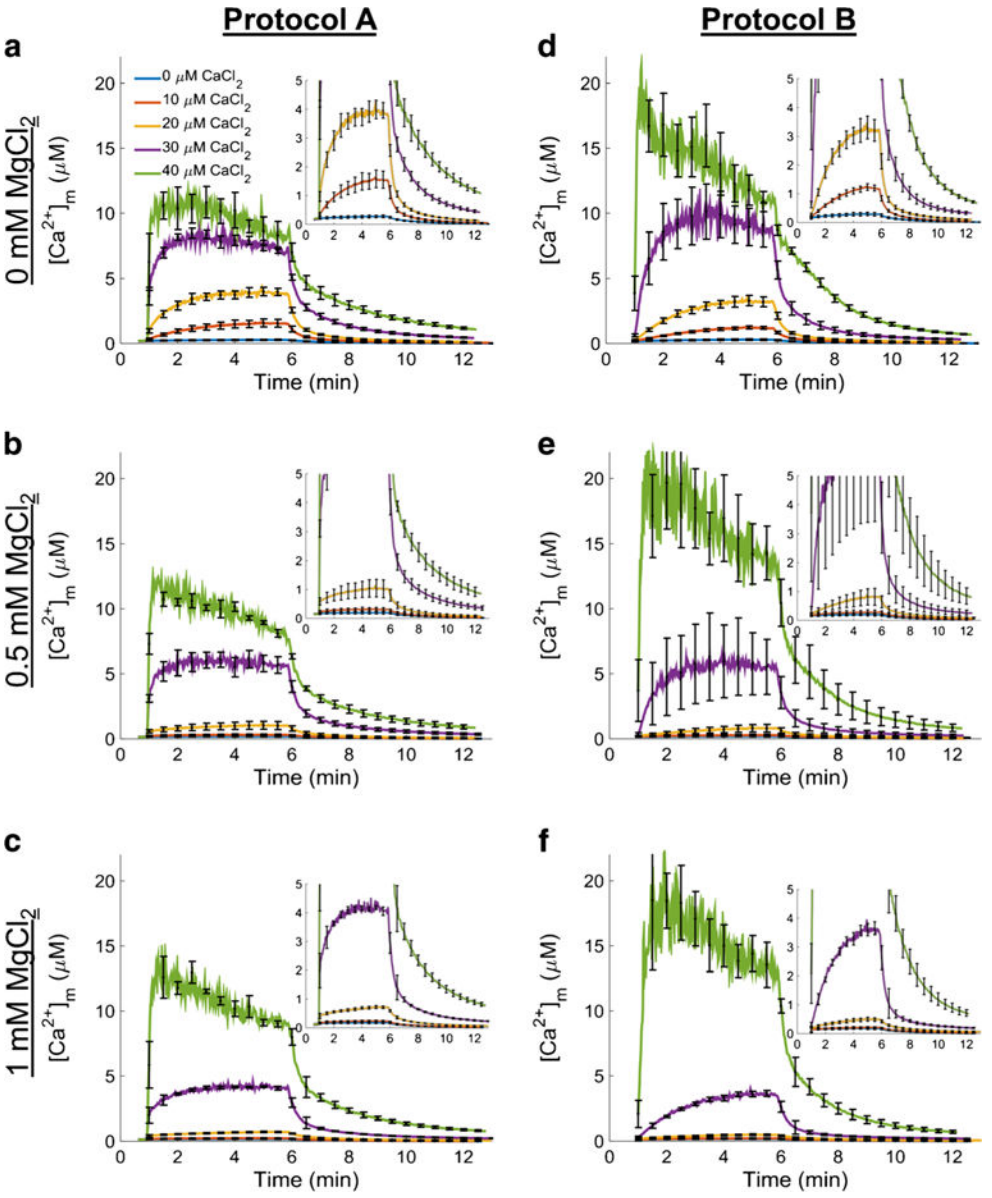

Fig. 4.

Matrix free Ca^{2+} ($[Ca^{2+}]_m$) dynamics. Ca^{2+} uptake and Ca^{2+} release for each combination of $CaCl_2$ and $MgCl_2$ concentrations are shown using the protocol depicted in Fig. 1. $CaCl_2$ was added to the respiring mitochondrial suspension (left column; protocol A) or mitochondria were added to the buffer containing a given $CaCl_2$ concentration (right column; protocol B) at 60 s followed by ruthenium red (RR) at 300 s and NaCl at 360 s. The results for protocol A are shown in the left column and the results for protocol B in the right column. In protocol B when $CaCl_2$ was 40 μM, the fluorescent signal was close to Rmax, so the calculated $[Ca^{2+}]_m$ is likely an overestimation of the true value of $[Ca^{2+}]_m$. Each row corresponds to the buffer $MgCl_2$ indicated on the left of each row. Insets show $[Ca^{2+}]_m$ dynamics for 0, 10, and 20 μM $CaCl_2$ in more detail. The axes are the same as the axes in the main figure panels. Error bars signify standard error of the mean

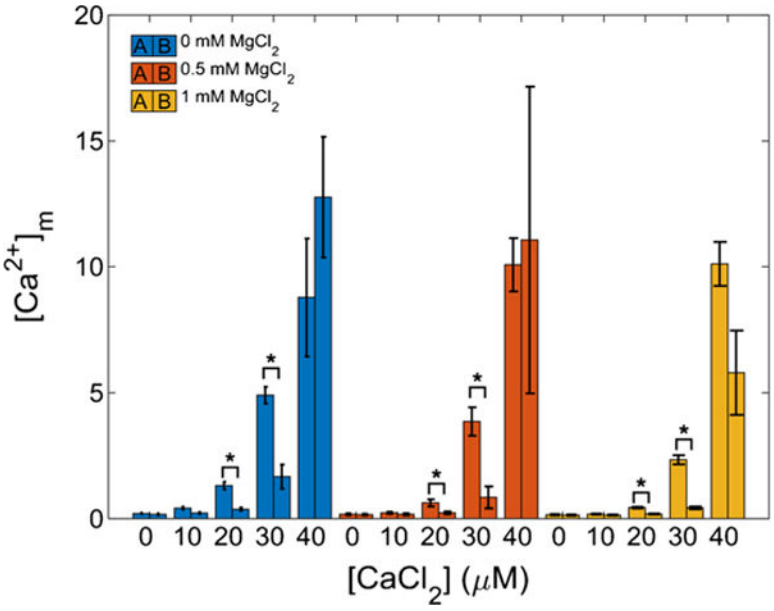

Fig. 5.

Ca^{2+} uptake by mitochondria. The amount of Ca^{2+} uptake by mitochondria depends on method of $CaCl_2$ delivery. The bar plots show $[Ca^{2+}]_m$ just after addition of $CaCl_2$ to mitochondria (protocol A, left bar) or after addition of mitochondria to buffer containing $CaCl_2$ (protocol B, right bar). These data correspond to a time of approximately 65 s. For all 20 and 30 μM $CaCl_2$ conditions, the rate of Ca^{2+} uptake in protocol A was significantly different from that of protocol B ($p \leq 0.05$) for most of the $[CaCl_2]$ and even in the presence of Mg^{2+}. Error bars signify standard error of the mean

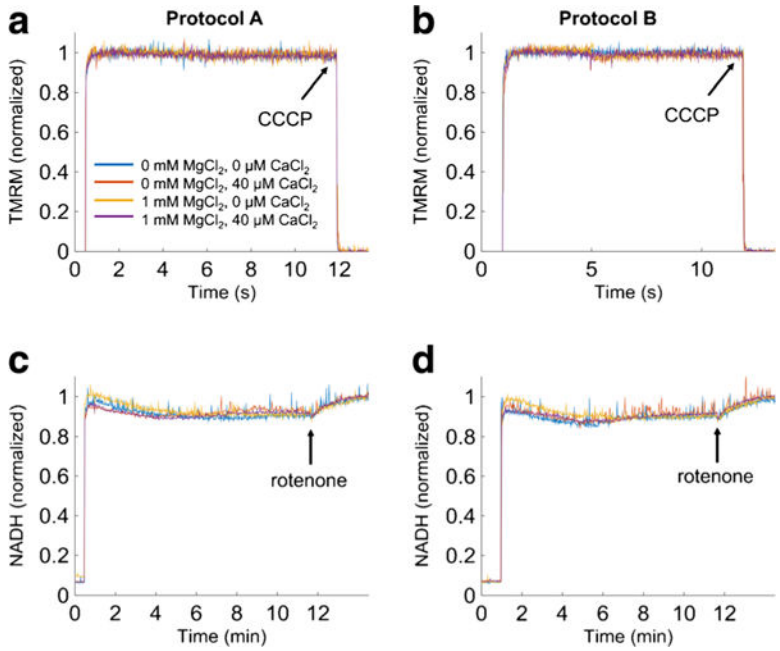

Fig. 6.

$\Delta\Psi_m$ and NADH dynamics. The bioenergetics responses during protocols A and B were monitored in parallel using the $\Delta\Psi_m$ sensitive dye TMRM and NADH autofluorescence. Traces are individual recordings. In averaged data there were no significant differences between the two $MgCl_2$ and $CaCl_2$ groups. The increases in signals mark the addition of mitochondria at 30 s (protocol A) and at 60 s (protocol B). The number of experimental groups was reduced to consist of only 0 and 1 mM $MgCl_2$ and 0 and 40 µM $CaCl_2$

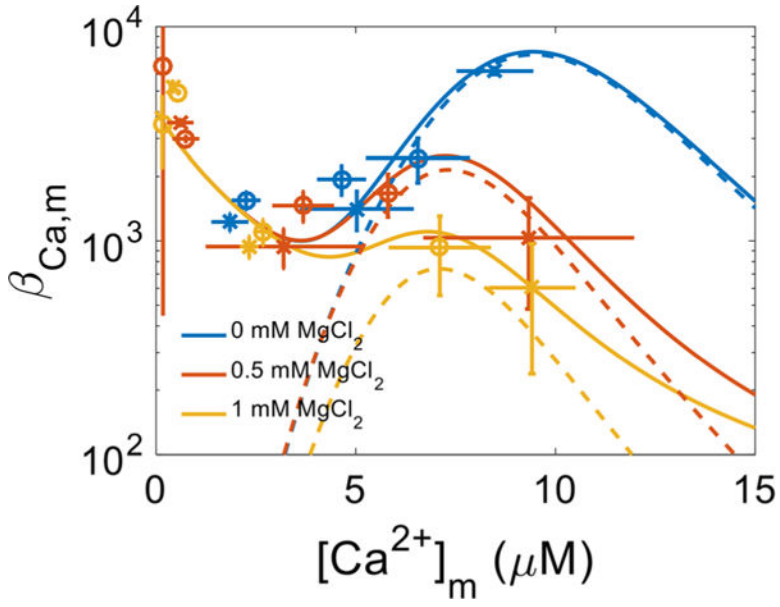

Fig. 7.

Mitochondrial Ca^{2+} buffering power. The Ca^{2+} sequestration system consists of at least two classes of buffers that bind Ca^{2+} with a differential affinity and capacity. Class 1 buffers are of the prototypical type whereby a single Ca^{2+} ion binds to a single site in an uncooperative manner. Class 2 buffers are atypical and bind multiple Ca^{2+} ions in a cooperative fashion. Class 1 buffers are not affected by Mg^{2+}; however, in the presence of Mg^{2+}, both the binding capacity and affinity of the Class 2 buffers are compromised. The blue, yellow and red colors correspond to the added 0 mM $MgCl_2$, 0.5 mM $MgCl_2$ and 1 mM $MgCl_2$ conditions, respectively. The circles (**O**) and x's (x) represent rates obtained using the data from Protocols A and B, respectively. The lines correspond to model simulations of the two classes of Ca^{2+} buffers using Eq. 2 with the parameters listed in Table 1. Error bars signify propagated standard deviations. Dashed lines represent contributions to mitochondrial buffering power from the class 2 buffers only

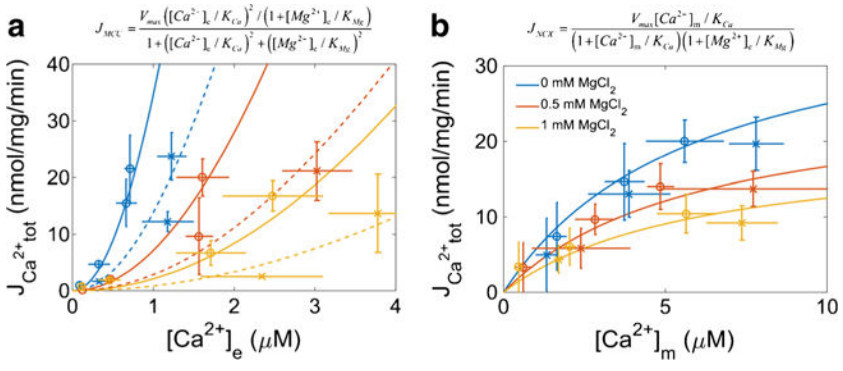

Fig. 8.

Mg^{2+} inhibition of Ca^{2+} uptake and extrusion. Panel 8a shows slow mode of Ca^{2+} uptake (via MCU) was attenuated by extra-matrix Mg^{2+} in the physiological concentration range. The model parameters for the simplified MCU model are: V_{max}, 900 nmol/mg/min; K_{Ca}, 6 μM; and K_{Mg}, 0.3 mM. Solid lines correspond to slow mode of MCU rates observed during protocol A, and dotted lines correspond to the slow mode of MCU rates observed during protocol B. The rates of Ca^{2+} uptake in protocol B were approximately 40 % of the rates observed in protocol A. Panel 8b shows buffer Mg^{2+} in the physiological range used in this study also affected the rate of Ca^{2+} efflux (via mNCE). The model parameters for the simplified NCE are: V_{max}, 40 nmol/mg/min; K_{Ca}, 5 μM; and K_{Mg}, 1 mM. The *blue, yellow* and *red* colors correspond to the 0 mM $MgCl_2$, 0.5 mM $MgCl_2$ and 1 mM $MgCl_2$ conditions, respectively. Extra-matrix $[Na^+]$ was assumed constant (10 mM) and thus not included in the equation. The circles (**O**) and x's (x) represent rates obtained using the data from Protocols A and B, respectively. The lines correspond to model simulations with the equations given above their respective panels. Error bars signify propagated standard deviations

Table 1

Mitochondrial Ca^{2+} sequestration system model parameters

Parameter	Definition	Value		
Class 1				
$[B_{Ca,1}]_{tot}$	Total Ca^{2+} buffer	12 mM		
$K_{Ca,1}$	Buffer Ca^{2+} affinity	3 μM		
n_1	Hill coefficient	1		
Class 2		0 Mg^{2+}	0.5 mM Mg^{2+}	1 mM Mg^{2+}
$[B_{Ca,2}]_{tot}$	Total Ca^{2+} buffer	8 mM	1.8 mM	0.6 mM
$K_{Ca,2}$	Buffer Ca^{2+} affinity	10 μM	7.75 μM	7.5 μM
n_2	Hill coefficient	6		